U. of Iowa 93-7

PLANETARY PLASMA WAVES

Donald A. Gurnett

January 1993

Submitted for publication in
Van Nostrand Reinhold's
The Encyclopedia of Planetary Sciences

Department of Physics and Astronomy
The University of Iowa
Iowa City, Iowa 52242

This research was supported by the National Aeronautics and Space Administration through Contract 959193 with the Jet Propulsion Laboratory.

I. An Introduction to Plasma Waves

A PLASMA IS an electrically neutral mixture of electrons and ions in which the kinetic energy greatly exceeds the interaction energy between the particles. Plasmas are produced (1) by collisions whenever a gas is heated to over a few thousand degrees, and (2) by photo-ionization, for example by ultraviolet radiation from the Sun. Plasmas are destroyed by recombination. Because of the very low densities that exist in interplanetary space and the correspondingly low recombination rates, almost all of the material that exists between the Sun and the planets is a plasma. This includes the solar corona, which is the hot ionized outer atmosphere of the Sun; the solar wind, which is an ionized gas streaming outward from the Sun at supersonic speeds; planetary magnetospheres, which are hot energetic plasmas surrounding planets with strong magnetic fields; and planetary ionospheres, which are layers of ionized gas in the upper regions of planetary atmospheres.

As in any fluid, waves can propagate through a plasma. Because of the electrical character of the plasma medium, plasma waves are very complex. Some of these waves have electric and magnetic fields, and are similar to the electromagnetic waves in free space. These are called electromagnetic waves. Others are more like sound waves and have no magnetic field. These are called electrostatic waves, since the electric field can be derived from the gradient of an electrostatic potential ($\bar{E} = -\bar{\nabla}\,\phi$). Usually, electromagnetic waves have propagation speeds near the speed of light, whereas electrostatic waves have propagation speeds near the speed of sound.

In most space plasmas the collision frequencies are very low. This type of plasma, with essentially zero collision frequency and infinite mean free path, is called a collisionless plasma. The absence of collisions effectively eliminates the basic mechanism of energy and momentum exchange that normally exists between particles in a fluid. Under this circumstance, waves provide the primary mechanism for energy and momentum exchange. Waves then play a role somewhat similar to collisions in an ordinary

gas. Whenever a sufficiently large deviation from thermal equilibrium occurs, waves grow spontaneously in the plasma. The nonequilibrium feature that gives rise to the wave growth is called a free energy source. Examples of free energy sources are beams and anisotropies in the velocity distribution of the particles. Once generated, the waves are eventually reabsorbed via a process known as collisionless damping. The wave growth and damping lead to an energy and momentum exchange. From very general principles it can be shown that the energy and momentum exchange acts to drive the plasma toward thermal equilibrium, very similar to collisions in an ordinary fluid. Waves, therefore, play a crucial role in maintaining the equilibrium state of the plasma.

Many different plasma wave modes exist in a plasma, particularly if the plasma has a magnetic field. These wave modes are usually associated with certain characteristic frequencies. The two primary characteristic frequencies of a plasma are the plasma frequency, ω_p, and the cyclotron frequency, ω_c. A plasma frequency and a cyclotron frequency can be defined for each species present in the plasma. The electron plasma frequency is given by

$$\omega_{pe} = \sqrt{\frac{e^2 n_e}{\epsilon_0 m_e}} \quad , \tag{1}$$

where e is the electronic charge, n_e is the electron number density, ϵ_0 is the permittivity of free space, and m_e is the electron mass. The electron plasma frequency is the characteristic oscillation frequency that occurs whenever electrons are perturbed from their equilibrium position in the plasma. The electron cyclotron frequency is given by

$$\omega_{ce} = \frac{eB}{m_e} \quad , \tag{2}$$

where B is the magnetic field. The electron cyclotron frequency is the characteristic rotation frequency that occurs whenever an electron has a component of velocity perpendicular to the magnetic field. Comparable equations for the ion plasma frequency and ion cyclotron frequency are obtained by changing

(e) to (i) in Equations 1 and 2. In addition to the electron and ion plasma frequencies and cyclotron frequencies, it is convenient to define four additional characteristic frequencies. These are: the upper hybrid resonance frequency,

$$\omega_{UHR} = \sqrt{\omega_{pe}^2 + \omega_{ce}^2} \quad , \tag{3}$$

the lower hybrid resonance frequency,

$$\omega_{LHR} = \sqrt{\omega_{ce}\,\omega_{ci}} \quad , \tag{4}$$

the right-hand cutoff,

$$\omega_{R=0} = \omega_{ce}/2 + \sqrt{(\omega_{ce}/2)^2 + \omega_{pe}^2} \quad , \tag{5}$$

and the left-hand cutoff,

$$\omega_{L=0} = -\omega_{ce}/2 + \sqrt{(\omega_{ce}/2)^2 + \omega_{pe}^2} \quad . \tag{6}$$

The relationships that these characteristic frequencies have to the various wave modes that exist in a plasma are summarized in Table 1. This table lists the commonly accepted name of the mode, the frequency range over which the mode can propagate, the electromagnetic/electrostatic character of the mode, the polarization (R,L) with respect to the magnetic field (when applicable), and the free energy source that can cause wave growth. It should be noted that Table 1 only applies to a plasma consisting of electrons and one positive ion species. If more than one positive ion species is present, then additional modes appear between adjacent pairs of ion cyclotron frequencies. For a further detailed discussion of the wave modes that can exist in a plasma, see Stix [1962] or Krall and Trivelpiece [1973].

II. INSTRUMENTATION

SPACE PLASMA WAVE MEASUREMENTS have been carried out by spacecraft-borne instrumentation for over thirty years. The first instruments specifically designed to study naturally occurring space plasma waves were launched on the Earth-orbiting Alouette 1 and Injun III satellites in 1962 [Barrington and Belrose, 1963; Gurnett and O'Brien, 1964]. Since then many different types of plasma wave instruments have flown on Earth-orbiting and interplanetary spacecraft. These instruments usually have several characteristics in common. In order to distinguish between electromagnetic waves and electrostatic waves, both electric and magnetic fields are usually measured. (The absence of a wave magnetic field indicates the wave is electrostatic.) Electric fields are usually detected by an electric dipole antenna that extends in opposite directions from the center of the spacecraft, as illustrated in Figure 1. The quantity measured is the voltage difference, $\Delta V = V_2 - V_1$, between the two antenna elements. The electric field component along the axis of the antenna is given by $E = \Delta V/\ell_{eff}$, where ℓ_{eff} is a quantity called the effective length. For wavelengths, λ, longer than the tip-to-tip length, L, of the antenna, the effective length is given by $\ell_{eff} = L/2$. A wide range of electric antenna lengths can be used, ranging from a fraction of a meter to over two hundred meters. Because the measured voltage ΔV increases with the antenna length, longer antennas are generally preferred, since they give better sensitivity. A variety of mechanisms are used to extend the antenna. One technique uses centrifugal force to pull a fine wire radially outward from a fishing-reel type of dispenser in the spacecraft. This technique only works on spinning spacecraft. Another technique uses a motor-driven device to extrude a thin metal tape through a guide to form a rigid metal tube. This type of antenna works equally well on both spinning and non-spinning spacecraft. Sometimes small metal spheres with internal high impedance amplifiers are placed on the ends of the antenna to sense the potential in the plasma [Fahleson, 1967]. In this case, the effective length is the center-to-center distance between the spheres.

Wave magnetic fields are usually detected using the magnetic induction principle, wherein a voltage is induced in a coil of wire by a time-varying magnetic field. The voltage induced is given by $V = Nd\Phi/dt$, where $\Phi = AB$ is the magnetic flux through the coil, N is the number of turns, A is the cross-sectional area, and B is the magnetic field. Two types of magnetic sensors are used. The first type is a loop antenna. Usually a loop antenna consists of a single turn, which minimizes the inductance and gives the maximum bandwidth. A transformer is usually used to couple the antenna to the electronics. The second type is a search coil magnetometer, which consists of a high-permeability rod surrounded by a sensing coil. The high-permeability rod acts to concentrate the magnetic flux through the coil, thereby increasing the sensitivity. Generally, loop antennas provide better sensitivities at higher frequencies, particularly above a few tens of kHz, whereas search coils provide better sensitivities at lower frequencies, below a few hundred Hz. To reduce interference from electrical systems on the spacecraft, magnetic field antennas are usually mounted on booms away from the spacecraft body, as illustrated in Figure 1. In some cases, multiple axis antennas are also used. Full three-axis measurements give information on the direction of propagation of a wave.

The signals from the electric and magnetic antennas can be processed in a variety of ways. A typical block diagram of a plasma wave instrument is shown in Figure 2. Usually the antennas are connected to preamplifiers located close to the antennas. The preamplifiers are designed to provide low noise levels and to optimize the transmission of signals from the antennas to the main electronics package. The frequency range over which the antenna/ preamplifier system must operate extends from the lowest characteristic frequencies of interest (usually f_{ci}) to the highest frequencies of interest (f_{pe} or f_{ce}). For planetary plasma wave investigations, this frequency range typically extends from a few Hz to a few MHz.

Two different techniques are employed to process signals from the electric and magnetic field sensors. In the first technique, an onboard spectrum analyzer is used to generate spectrum amplitudes at a series of frequencies, f_1, f_2, ..., f_n. A spectrum analyzer of this type is shown in the top portion of the

block diagram in Figure 2. The purpose of the onboard spectrum analysis is to provide continuous low-resolution survey spectrums using relatively modest telemetry rates, typically a few hundred bits/s. In the second technique, a wideband receiver is used to transmit electric or magnetic field waveforms directly to the ground. The onboard signal processing is minimal, and the spectrum processing (Fourier analysis) is performed by ground-based computers.

A wideband receiver is shown at the bottom of the block diagram in Figure 2. The main purpose of the wideband receiver is to limit the bandwidth of the signal and to control the amplitude of the signal by means of an automatic gain control. The waveform transmission can be either analog or digital. The advantage of the waveform measurements is the very high resolution. Since the entire waveform is transmitted, the resolution in frequency and time is limited only by the uncertainty principle ($\Delta\omega\Delta t \simeq 1$). The disadvantage is that the telemetry rates are extremely high, often several hundred kbits/s or more. For this reason, wideband waveform transmissions are often of limited duration (60 sec or less), thereby restricting the waveform measurements to a few specific samples, rather than continuous coverage. In this respect, the onboard spectrum analysis and the wideband technique are complementary. The spectrum analyzer provides continuous low-resolution survey measurements, and the wideband receiver provides high-resolution spectrums for selected time intervals.

III. OBSERVATIONS

SPACECRAFT PLASMA WAVE observations have now been obtained at seven planets (Venus, Earth, Mars, Jupiter, Saturn, Uranus, and Neptune). The most extensive measurements have been performed in the vicinity of Earth. Since the first such measurements in 1962 many spacecraft have provided plasma wave measurements in Earth orbit. These spacecraft have explored most of the near-Earth environment, with trajectories ranging from low altitude orbits near the Earth's surface, to highly eccentric orbits extending well beyond the orbit of the Moon. The plasma wave observations at the other planets are much more limited, and it is these measurements that will be emphasized here, since they are at the frontier of present day research. Of the various spacecraft that have flown to the other planets, the Voyager 1 and 2 mission to the giant planets, Jupiter, Saturn, Uranus, and Neptune, has probably contributed the most to our expanding knowledge of space plasma waves. The giant planets, like the Earth, have strong magnetic fields and intense radiation belts, which makes them a rich source of plasma waves. For the initial Voyager reports of plasma wave observations at the giant planets, see Scarf et al. [1979a; 1982] and Gurnett et al. [1979a; 1981; 1986; 1989]. The only other spacecraft that has provided plasma wave measurements at the giant planets is Ulysses, which flew by Jupiter in 1992. For the initial report of the Ulysses plasma wave observations, see Stone et al. [1992]. The remaining two planets, Venus and Mars, have negligible internal magnetic fields and therefore fewer types of plasma wave phenomena. The first measurements of plasma waves in the vicinity of Venus were provided by the Pioneer-Venus spacecraft, which was placed in orbit around Venus on December 4, 1979. The first report on the Pioneer-Venus plasma wave observations was given by Scarf et al. [1979b]. The only other spacecraft that has provided plasma wave observations in the vicinity of Venus is Galileo, which flew by Venus on February 10, 1990. For a report on the Galileo-Venus plasma wave observations, see Gurnett et al. [1991]. At Mars the first, and only, plasma wave measurements were obtained by the Phobos 2 spacecraft, which was

placed in orbit around Mars on January 29, 1989. An initial report on the Phobos 2 plasma wave observations is given by Grard et al. [1991].

Since there are so many planets to review, no attempt will be made to describe the observations in detail at each planet. Instead, the observations will be organized according to the various types of plasma waves observed, ordered according to decreasing distance from the planet, starting from the sunward side of the planet, and ending in the region near the closest approach. No discussion is given of electromagnetic radiation that can escape to great distances from the planet, since these waves are usually regarded as radio astronomical emissions. For a review of planetary radio emissions see Gurnett [1992].

A. Electron Plasma Oscillations and Ion Acoustic Waves

The solar wind flows outward from the Sun at a nearly constant speed of about 400 km/s. At this speed the solar wind flow is supersonic. When the solar wind encounters a large object such as a planet, a shock wave is formed, very similar to the shock wave that forms upstream of an airplane in supersonic flight. This shock is called the bow shock. The approximate shape of the shock is shown in Figure 3. If the planet has no internal magnetic field, as in the case

of Venus and Mars, the planet and its surrounding atmosphere and ionosphere act as the obstacle. The radial distance to the nose of the shock is then only slightly larger than the radius of the planet. If the planet has a strong internal magnetic field, as in the case of the Earth and the giant planets, then the magnetic field acts as the obstacle. The position of the shock is then controlled by the strength of the planetary magnetic field. The interface between the solar wind and the planetary magnetic field is called the magnetopause (see Figure 3). At Jupiter, for example, the nose of the shock is typically at 80 to 120 R_J (where R_J is the radius of the planet), and the magnetopause is at 50 to 70 R_J.

At the shock, the plasma is strongly heated and some of the electrons and ions escape upstream into the solar wind. Because the backstreaming particles are guided along the magnetic field lines by

magnetic forces, these particles are confined to a region upstream of the shock called the foreshock. Usually the escaping electrons have very high speeds, typically 10^4 to 10^5 km/s, which is much greater than the solar wind speed. At these very high velocities, the region accessible to the backstreaming electrons is essentially delineated by the magnetic field lines tangent to the shock (see Figure 3). This region is called the electron foreshock. The escaping ions, because of their higher mass, have much lower velocities, more nearly comparable to the solar wind speed. The region accessible to the backstreaming ions is therefore angled backward substantially from the tangent field line (see Figure 3). This region is called the ion foreshock.

Because the backstreaming electrons constitute a beam, these particles can excite electron plasma oscillations, also sometimes called Langmuir waves (see Table 1). Electron plasma oscillations excited by electrons streaming into the solar wind were first discovered by Scarf et al. [1971] upstream of the Earth's bow shock. Since then similar electron plasma oscillations have been discovered at Venus and Mars and at all four of the giant planets. A multi-channel plot illustrating the occurrence of electron plasma oscillations upstream of Jupiter's bow shock is shown in Figure 4. These data are from the low-rate spectrum analyzer onboard Voyager 1. The enhanced emissions in the 5.62-kHz channel from about 1218 to 1227 UT are electron plasma oscillations. The electron plasma frequency, f_{pe}, during this interval was about 5.5 to 6.0 kHz. The onset of the plasma oscillations at 1218 UT corresponds to the crossing of the tangent field line, and the termination at 1227 UT corresponds to the crossing of the bow shock.

The frequency of upstream electron plasma oscillations generally decreases with increasing distance from the Sun. As can be seen from Equation 1, the electron plasma frequency is proportional to the square root of the electron density. Since the solar wind density varies roughly as $1/R^2$, where R is the distance from the sun, the electron plasma frequency varies roughly as 1/R. At Venus the electron plasma frequency is typically about 30 kHz, whereas at Neptune the electron plasma frequency is about 700 Hz. The electric field strength of the plasma oscillations also decreases with increasing distance from

the Sun. At Venus and Earth, the peak field strengths are about 1 mV/m, whereas at Neptune the peak field strengths are about 30 to 100 μV/m.

In addition to electron plasma oscillations, another type of wave also occurs upstream of planetary bow shocks. These waves were first detected upstream of the Earth's bow shock by Scarf et al. [1970] and are called ion acoustic waves [Gurnett and Frank, 1978]. The ion acoustic waves are very similar to sound waves in an ordinary gas and are driven by ions escaping from the shock. Since these waves are driven by ions, they are confined to the ion foreshock. A wideband spectrogram of ion acoustic waves detected by the Voyager 1 spacecraft upstream of Jupiter's bow shock is shown in Figure 5. As can be seen, the ion acoustic waves have relatively narrow bandwidths and switch on and off abruptly. The abrupt onsets and terminations indicate that the mode is very close to marginal instability. The peak frequencies of the ion acoustic waves ($\sim$2 kHz) are well below the electron plasma frequency ($f_{pe} \sim 5$ kHz) but still above the ion plasma frequency ($f_{pi} \sim 120$ Hz). As can be seen from Table 1, the ion acoustic mode can only propagate at frequencies below the ion plasma frequency. This discrepancy is believed to occur because the waves have very short wavelengths, thereby introducing Doppler shifts due to the motion of the solar wind. For a wave of wavelength λ and frequency f in the plasma rest frame, the frequency f' detected in the spacecraft rest frame is given by

$$f' = f + \frac{V_{sw}}{\lambda} \cos \theta_{kv} \quad , \tag{7}$$

where V_{sw} is the solar wind speed and θ_{kv} is the angle between the propagation vector $\vec{k}$ and the solar wind velocity. The shortest wavelength that can exist in a plasma is $\lambda_{min} = 2\pi\lambda_D$, where λ_D is a characteristic length called the Debye length. For the plasma parameters that exist in the solar wind upstream of Jupiter, the shortest wavelength is about $\lambda_{min} \simeq 240$ m. The maximum Doppler shift, which is given by the second term on the right-hand side of Equation 3, is then about 1.7 kHz, which is comparable to the highest frequencies observed. Ion-acoustic waves have only been reported upstream of the bow shocks at Earth, Mars, and Jupiter. For unknown reasons, possibly due to instrumental

limitation, ion acoustic waves have not been observed upstream of the bow shocks at Venus, Saturn, Uranus, or Neptune.

The bow shock crossings at Venus, Earth, Mars, and all four of the giant planets can be easily identified in the plasma wave data by an intense broadband burst of electric field noise at the shock. This noise was first discovered in the Earth's bow shock by Fredricks et al. [1968]. A wideband frequency-time spectrogram showing the shock-related electric field noise observed during the Voyager 1 crossing of Jupiter's bow shock is given in Figure 6. This is the same shock crossing shown in Figure 4. Note the electron plasma oscillations at ~ 6 kHz, increasing slowly in frequency as the spacecraft approaches the shock. The electric field noise at the shock extends up to a frequency of about 3 kHz and has a peak broadband intensity of about 1 mV/m. This noise is believed to be caused by solar wind ions that are magnetically reflected by the shock, thereby forming a gyrating ion beam that excites electrostatic waves via a two-stream instability. Currents flowing along the shock surface may also in some cases contribute to the generation of electrostatic waves. Earlier it was thought that the electric field noise played the dominant role in heating the plasma at collisionless shocks [Fredricks et al., 1968]. However, more recent studies by Scudder et al. [1986] and others suggest that the electric field noise probably acts only to thermalize the particle distribution, and that other processes, such as acceleration by quasi-static electric fields and magnetic reflection, are primarily responsible for converting the directed solar wind flow into a heated distribution at the shock.

B. Trapped Continuum Radiation

After the shock, the next boundary to be crossed by a spacecraft approaching from the sunward side of the planet is the magnetopause. This boundary forms the effective obstacle for the solar wind flow around the planet and is shown by a dashed line in Figure 3. Because the planetary magnetic field provides most of the pressure inside of the magnetosphere, an abrupt drop in the plasma density occurs at the magnetopause, thereby forming a low-density magnetospheric cavity. Since the electron plasma

frequency is lower in the magnetosphere than in the solar wind, electromagnetic radiation can be trapped in the magnetospheric cavity. This trapped radiation was first discovered in the Earth's magnetosphere by Gurnett and Shaw [1973] and is called continuum radiation. Since then, trapped continuum radiation has been observed at three of the giant planets, Jupiter, Saturn, and Uranus. No trapped continuum radiation was observed at Neptune, probably because the Voyager plasma wave instrument did not have sufficient sensitivity to detect this radiation at Neptune. The trapped continuum radiation at Jupiter is particularly intense and is one of the most intense emissions observed at any of the planets. Since no magnetospheric cavity exists at Venus and Mars, trapped continuum radiation cannot occur at either of these planets. For a review of continuum radiation in planetary magnetospheres see Kurth [1991].

An example of trapped continuum radiation is shown in Figure 7. This spectrogram shows the Voyager 1 crossing of the magnetopause at Jupiter. The continuum radiation consists of the dark band of noise extending upward from about 1 kHz, gradually fading into the receiver background noise above about 7 kHz. The sharp, low-frequency cutoff of the radiation is believed to be caused by the reflection of free space (L,O) mode electromagnetic waves at the local electron plasma frequency. As can be seen from Table 1, the free space L,O mode can only propagate at frequencies $f > f_{pe}$. Free-space (R,X) mode radiation is also most likely present. However, the low frequency cutoff of the R-X mode is always above f_{pe}, so the L-O mode always determines the low-frequency cutoff. The monotonic decrease in the low frequency cutoff, from about 6.2 kHz to 1.8 kHz, over a period of about 20 seconds, is caused by the rapidly declining plasma density as the spacecraft passes through the magnetopause. Note from Equation 1 that the electron plasma frequency is proportional to the square root of the electron density. The thickness of the magnetopause is controlled mainly by the cyclotron radius of magnetosheath ions as they gyrate into the region of strong field inside the magnetosphere. Continuum radiation comparable to Figure 6 is observed throughout the magnetospheric cavity of Jupiter. Once generated, the radiation is believed to undergo repeated reflections from the walls of the cavity, eventually building up to an equilibrium level throughout the cavity. Small, random Doppler shifts caused by repeated reflections from the walls of the

magnetospheric cavity, which are continuously in motion, are believed to spread the radiation into a nearly continuous spectrum, hence the term continuum.

C. Electron Cyclotron and Upper Hybrid Waves

For the magnetized planets, the magnetic field within the magnetosphere is generally much stronger than in the solar wind. The electron cyclotron frequency then plays an important role in controlling the types of waves that are generated. In the Earth's magnetosphere, it has been known for many years that strong electrostatic emissions are generated near harmonics of the electron cyclotron frequency [Kennel et al., 1970; Shaw and Gurnett, 1975]. These emissions are part of a band structure that is often referred to as electron cyclotron waves (see Table 1). The free energy source of these waves consists of electrons with a loss-cone or ring-type of distribution function. Loss-cone velocity distributions are a characteristic feature of planetary radiation belts. Charged particles moving within a well-defined cone of angles around the magnetic field (the loss cone) strike the atmosphere and are lost from the system, thereby producing a hole in the particle velocity distribution.

Electron cyclotron waves are found in the magnetosphere of the Earth and all the giant planets. Typically these waves are most intense near half-integral harmonics $(n + 1/2)f_{ce}$ of the electron cyclotron frequency. Usually the $(n + 1/2)f_{ce}$ waves occur in two distinct frequency ranges, the first near low-order half-integral harmonics of the electron cyclotron frequency (i.e., $(3/2)f_{ce}$, $(5/2)f_{ce}$, etc.), and the second near the upper hybrid resonance frequency, when $(n + 1/2)f_e \simeq f_{UHR}$. The low-order harmonics are often called electron cyclotron harmonic (ECH) waves, and the emissions near the upper hybrid frequency are called upper hybrid resonance (UHR) waves. The emission frequencies depend in a complicated way on the densities and temperatures of the cold and hot components of the plasma, and are almost never exactly at $(n + 1/2)f_{ce}$. The half-integral notation, 3/2, 5/2, etc., is mainly just a convenient label to identify the emission band.

A spectrogram illustrating examples of low-order (3/2, 5/2, and 7/2) ECH emissions in the magnetosphere of Saturn is shown in Figure 8. The emission frequencies in this case are slightly above the electron cyclotron harmonics. Considerable fine structure can be seen within the emission bands. Electron cyclotron harmonic emissions of this type are typical of all the ECH observations at the giant planets. Usually, the emissions are strongest in a narrow band slightly above the electron cyclotron harmonics. A spectrogram illustrating an example of UHR emissions in the outer region of Jupiter's magnetosphere is shown in Figure 9. The UHR emissions in this case consist of very sharply defined bands near the lower edge of the trapped continuum radiation. The bands switch on and off as plasma density variations cause the upper hybrid resonance frequency to sweep past half-integral harmonics of the electron cyclotron frequency. Strong emissions occur whenever the condition $(n + 1/2)f_{ce} \simeq f_{UHR}$ is satisfied. The frequency spacing between the bands is roughly the electron cyclotron frequency.

A striking characteristic of both the ECH and UHR waves is their close confinement to the magnetic equator. The top panel of Figure 10 shows a multi-channel plot of electric field intensities from the Voyager 1 pass through the inner region of the Jovian magnetosphere. The ECH and UHR emissions are identified by circles. The bottom panel shows the magnetic latitude, λ_m. The magnetic latitude oscillates up and down due to the rotation of Jupiter's magnetic dipole field, which is tilted at an angle of about 10° with respect to the rotational axis. As can be seen the ECH and UHR waves occur in sharply localized regions centered almost exactly on the magnetic equator crossings. This narrow confinement to a region only one or two degrees from the magnetic equator is a characteristic feature of all the ECH and UHR observations at the giant planets. A similar effect also occurs in the Earth's magnetosphere, although not as dramatic as at the giant planets.

The reason that the ECH and UHR waves are confined to a narrow region near the magnetic equator is still a subject of investigation. Based on terrestrial studies it is believed that two factors are responsible. First, it is known that the electrons responsible for generating the waves have pitch angles near 90°. Due to the laws governing the motion of trapped radiation belt particles (conservation of the

first and second adiabatic invariants), particles with pitch angles near 90° are closely confined to the vicinity of the magnetic equatorial plane. Since highly anisotropic pancake-like velocity distributions are required to generate the ECH and UHR waves, large wave growth can only occur near the magnetic equator. Second, ray tracing studies show that the electron cyclotron waves tend to be guided along the magnetic equator. This guiding effect is believed to further confine the wave growth to a narrow region along the magnetic equatorial plane.

One may ask what role these waves play in the magnetospheres of the giant planets. In the terrestrial magnetosphere, electron cyclotron waves have for many years been thought to play a role in the loss of trapped radiation belt electrons by scattering particles into the loss cone [Kennel et al., 1970]. It seems likely that similar processes are operative at the giant planets. Unfortunately, adequate measurements are not available from the Voyager plasma data in the proper electron energy range (a few hundred eV to several tens of keV) to evaluate this loss mechanism. In the Earth's magnetosphere, UHR emissions are also believed to be a source of free space electromagnetic radiation. The generation mechanism is believed to involve a mode conversion process by which UHR waves are converted to escaping electromagnetic (L,O mode) radiation. The mode conversion process can be either linear [Jones, 1980] or nonlinear [Melrose, 1981]. Trapped continuum radiation is thought to be produced by this mode conversion process [Kurth, 1991].

D. Whistler-Mode Emissions

Whistlers are one of the oldest and best known terrestrial plasma wave phenomena. Whistlers were first observed by ground-based radio receivers [Barkhausen, 1919]. The modern theory of whistlers was first proposed by Storey [1953]. According to Storey's theory, low-frequency electromagnetic radiation from a lightning discharge is guided along the magnetic field lines through the magnetospheric plasma. Because of the peculiar nature of electromagnetic wave propagation at frequencies below the electron cyclotron frequency, the higher frequencies propagate faster than the lower frequencies. Thus,

the broadband impulsive signal produced by a lightning flash is converted into a whistling tone, hence the term "whistler". The plasma wave mode involved in the propagation of whistlers is called the whistler mode. Whistler mode waves are right-hand polarized and propagate at frequencies below either f_{ce} or f_{pe}, whichever is smaller (see Table 1). The whistler mode is highly anisotropic and has a number of unusual characteristics, one of which is that the index of refraction goes to infinity along a cone of directions called the resonance cone [Stix, 1962]. This highly anisotropic characteristic accounts for the fact that the wave energy is guided approximately along the magnetic field lines. For a further discussion, see the entry on Whistlers [this volume, 1993].

In addition to lightning-generated whistlers, whistler-mode waves are also spontaneously generated in magnetized plasmas. These waves are called whistler-mode emissions. Whistler-mode emissions are a common feature of the terrestrial magnetosphere and occur in the magnetospheres of all the giant planets. These emissions are mainly generated in the inner regions of the magnetosphere where the loss-cone in the trapped energetic electron distribution provides an effective free energy source. From very general principles [Brice, 1964], it can be shown that the growth of whistler-mode waves leads to a decrease in the pitch angle of resonant electrons, thereby driving the particles toward to the loss cone. The growth of whistler-mode waves is widely believed to be the dominant mechanism responsible for the loss of energetic electrons from planetary radiation belts. In a classic paper, Kennel and Petschek [1966] showed that the growth of whistler-mode waves puts an upper limit on the energetic electron intensities that can exist in planetary radiation belts.

A representative spectrum of whistler-mode emissions in the inner region of Jupiter's magnetosphere is shown in the top panel of Figure 11. This spectrum was obtained in the Io plasma torus, which is a dense torus of plasma produced by gases escaping from Jupiter's moon Io (see the entry on Planetary Tori, [this volume, 1993]). The plasma in the Io torus is extremely energetic and produces very intense whistler-mode emissions, among the most intense ever observed in a planetary magnetosphere. Two types of emissions are observed, called "hiss" and "chorus". The hiss is an essentially structureless

emission. When the hiss signals are played through an audio speaker, they make a steady hissing sound, hence the term "hiss." According to current ideas, whistler-mode hiss is believed to represent a fully developed turbulent spectrum in which the wave growth and loss has achieved a steady state equilibrium. In contrast to the whistler-mode hiss, chorus emissions are highly structured. A wideband frequency-time spectrogram of chorus is shown in Figure 12. The term "chorus" is an old term [Allcock, 1957], and has its origins in the term "dawn chorus" which refers to the sounds made by a roosting flock of birds at daybreak. The reasons for the complex spectral structure, usually consisting of many discrete narrowband tones rising in frequency, is poorly understood. The current view is that the waves grow to large amplitudes so rapidly that local nonlinear processes play a dominant role in controlling the evolution of the wave. Computer simulations show that particles trapped in the wave field produce isolated wave packets, each of which evolves somewhat differently in time and space.

It is instructive to comment on the electron energies involved in the generation of hiss and chorus. Whistler-mode wave growth proceeds via a resonant process in which a constant force is experienced by a particle undergoing cyclotron motion along a magnetic field line, thereby leading to a deceleration (or acceleration) of the particle and a growth (or damping) of the wave. This process is called cyclotron resonance. The general condition for cyclotron resonance is

$$v_{\parallel Res} = \frac{\omega - n\,\omega_{ce}}{k_{\parallel}} \quad , \tag{8}$$

where $v_{\parallel Res}$ is the parallel resonance velocity (the symbol " $\parallel$ " refers to the component parallel to the magnetic field), ω is the wave frequency, $k_{\parallel}$ is the parallel component of the wave vector, and n is an integer. For whistler-mode waves, the n = 1 term is usually most important. This resonance is called the first-order cyclotron resonance and occurs when both the wave and the particles (electrons) are rotating in the right-hand sense with respect to the magnetic field. From the propagation characteristics of the wave, $\omega(k)$, one can calculate the parallel energy, $W_{\parallel}$, of the resonant electrons. The parallel resonance

energy for whistler-mode emissions at Jupiter is shown in the bottom panel of Figure 11. As can be seen, the resonance energy decreases rapidly with increasing frequency. The energy of the electrons interacting with the hiss tends to be very high, 100 to 1000 keV, whereas the energy of the electrons interacting with the chorus tends to be much lower, 1-10 keV. This trend, for hiss to resonate with high energies and chorus to resonate with low energies, is typical of whistler-mode emissions at all of the giant planets.

In addition to Earth, three of the giant planets, Jupiter, Saturn, and Uranus, have intense whistler-mode hiss and chorus emissions. These emissions occur in the inner regions of the magnetosphere where the trapped radiation belt electron intensities are the highest. The existence of whistler-mode emissions at Neptune is unclear. Some very weak emissions were observed in the low-rate data that are probably whistler-mode hiss. However, no chorus was observed in any of the wideband data. The absence of chorus at Neptune could be due to the low radiation belt intensities, which were the lowest of any of the giant planets. It can be shown that the growth rate of whistler-mode emissions increases in direct proportion to the intensity of the resonant electron. The extremely low whistler-mode emission intensities at Neptune could therefore be due to the low radiation belt electron intensities. On the other hand, the spacecraft did not pass through the equatorial region of the radiation belt where the highest wave amplitudes would be expected. Thus, it may be that strong whistler-mode emissions were present in the magnetosphere of Neptune, but the spacecraft did not pass through the proper region to observe these waves.

A third type of whistler-mode emission also occurs in planetary magnetospheres. This emission occurs in the auroral regions and is called auroral hiss. Auroral hiss is a nearly structureless emission and is believed to propagate at wave normal angles near the resonance cone. Near the resonance cone the whistler mode is very nearly electrostatic, with small magnetic fields, short wavelengths, and low propagation speeds. These short wavelength quasi-electrostatic whistler mode waves are sometimes called lower hybrid waves, since they become completely electrostatic at the lower-hybrid resonance frequency, f_{LHR}. Because of the low propagation velocity, auroral hiss can be excited by beams, very similar to

electron plasma oscillations. Auroral hiss has been extensively studied in the Earth's magnetosphere, where it has been shown that the emissions are produced by the same electron beams that produce the auroral light emission, hence the term "auroral hiss." Auroral hiss has also been observed at Jupiter by Voyager 1 [Gurnett et al., 1979b], and by Ulysses [Stone et al., 1992]. In both cases the identification was based on the similarity to terrestrial auroral hiss and not on a direct correlation with the aurora on Jupiter. No auroral hiss was observed at Saturn, Uranus, or Neptune, most likely because the spacecraft did not pass through the proper region to observe such emissions.

E. Electrostatic Ion Cyclotron Waves

Electrostatic ion cyclotron waves occur in discrete bands between harmonics of the ion cyclotron frequency (see Table 1), very similar to electron cyclotron waves, which occur between harmonies of the electron cyclotron frequency. One of the unique features of the electrostatic ion cyclotron mode is that it is driven unstable by relatively weak field line currents. This feature led Kindel and Kennel [1971] to predict that electrostatic ion cyclotron waves would be produced by field-aligned currents over the Earth's auroral regions. The existence of such waves was subsequently confirmed by Kintner et al. [1978], using data from the polar orbiting S3-3 satellite. A representative spectrum of electrostatic ion cyclotron waves observed along the Earth's auroral field lines is shown in Figure 13. Strong enhancements can be seen just above the lowest three harmonics of the proton (H^+) cyclotron frequency. Originally it was thought that these waves were driven by field-aligned currents. However, more recent studies suggest that these waves are produced by ion beams accelerated upward along the auroral field lines by the same quasi-static electric fields that produce the electron precipitation responsible for the aurora. Electrostatic ion cyclotron waves are also sometimes observed near the magnetic equatorial plane. These waves are believed to be driven by energetic ions trapped near the magnetic equator.

Observations of electrostatic ion cyclotron waves in other planetary magnetospheres are very limited. Since the Voyager spacecraft did not pass through the high latitude auroral regions at the giant

planets, with the possible exception of Neptune, no opportunity existed to search for electrostatic ion cyclotron waves driven by auroral processes. Barbosa and Kurth [1990] have interpreted a narrow band of low frequency waves observed in the cold plasma torus at Jupiter as electrostatic ion cyclotron waves. They suggest that these waves are produced by a charge exchange interaction between neutral gas emissions from volcanos on Io and the rapidly rotating Io plasma torus, which is locked to the rotation of Jupiter. This charge exchange process produces a ring-type ion distribution (sometimes called pick-up ions) and is expected to provide a very effective free energy source for generating electrostatic ion cyclotron waves. Barbosa et al. [1990] have also interpreted a band of low frequency electric field noise in Neptune's magnetosphere as electrostatic ion cyclotron waves, also driven by the same charge exchange process. Unfortunately, in neither case is it possible to confirm the electrostatic character of the waves, so the identification of the mode is not completely certain.

F. Electromagnetic Ion Cyclotron Waves

Electromagnetic ion cyclotron waves are very similar to whistler mode waves, except that they are left-hand polarized and propagate below the ion cyclotron frequency (see Table 1). Since the ion cyclotron frequency is much lower than the electron cyclotron frequency (see Equation 2), ion cyclotron waves necessarily occur at extremely low frequencies, typically a few hundred Hz or less. Since the wave field of an electromagnetic ion cyclotron wave rotates in the same sense as positive ions (i.e., left-hand with respect to the magnetic field), these waves interact strongly with positively charged ions. Almost all of the ions observed in planetary magnetospheres are positively charged. The cyclotron resonance condition is identical to Equation 8, except that (e) is replaced by (i). Electromagnetic ion cyclotron waves are driven unstable by a loss-cone in the energetic ion distribution. Since a loss cone is always present in a planetary radiation belt, the growth of these waves provides a mechanism for scattering energetic ions into the loss cone, thereby controlling the loss of radiation belt ions.

Despite the intense theoretical interest in the generation of electromagnetic ion cyclotron waves in planetary magnetospheres, relatively few observations are available. The first report of spontaneously generated electromagnetic ion cyclotron waves in the Earth's magnetosphere was by Taylor et al. [1975]. These and other subsequent observations [Kintner et al., 1977; Roux et al., 1982] have shown that electromagnetic ion cyclotron waves are generated in the Earth's radiation belt during magnetic storms, when intense fluxes of energetic (10 to 100 keV) ions are injected deep into the inner regions of the magnetosphere. Electromagnetic ion cyclotron waves have also been observed at Jupiter by Thorne and Scarf [1984] using Voyager 1 measurements, and by Stone et al. [1992] using Ulysses measurements. In both cases, intense waves were observed at frequencies below the proton cyclotron frequency. The Ulysses observations are particularly important because the magnetic field of the wave was measured, which confirms that the waves are electromagnetic and not electrostatic (Voyager had only an electric antenna). The ion precipitation produced by these waves is believed to be responsible for the extreme ultraviolet (EUV) aurora at Jupiter [Thorne and Moses, 1983]. Using Voyager 2 Neptune data, Gurnett et al. [1989] reported observations of a strong band of electric field noise at Neptune at frequencies below the proton cyclotron frequency. This band of electric field noise was tentatively identified as electromagnetic ion cyclotron waves. However, since no wave magnetic field measurements were available, it was not possible to definitely establish the mode of propagation.

III. CONCLUSION

THIS REVIEW HAS DESCRIBED the primary types of plasma waves observed in the vicinity of the planets Venus, Mars, Earth, Jupiter, Saturn, Uranus, and Neptune. These observations are summarized in Table 2. By necessity we have not attempted to describe the detailed nature of the observations at each planet. For a more detailed description, see the review by Kurth and Gurnett [1991]. In making comparisons between these planets it must be recognized that the observations are in many cases incomplete, particularly at Uranus and Neptune where the available data are limited to only one pass by the planet. At the giant planets almost no information is available at high magnetic latitudes, a region that we know from terrestrial observations has many complex auroral-related plasma wave emissions. No plasma wave observations have been obained at Mercury and Pluto. Thus, there are very significant gaps in our knowledge. It is likely to be many years before these gaps are filled. The most promising missions for future plasma wave investigations are Galileo, which is to orbit Jupiter in late 1995, and Cassini, which is to orbit Saturn early in the next century. Both of these spacecraft include plasma wave instruments.

ACKNOWLEDGEMENTS

THIS RESEARCH WAS SUPPORTED by NASA through contract 959193 with the Jet Propulsion Laboratory.

REFERENCES

Allcock, G. Mck., 1957, A study of the audio-frequency radio phenomena known as "dawn chorus," *Australian J. Phys.* **10**, 286.

Barbosa, D. D., and W. S. Kurth, 1990, Theory and observations of electrostatic ion waves in the cold ion torus, *J. Geophys. Res.* **95**, 6443.

Barkhausen, H., 1919, Zwei mit Hilfe der neuen Verstärker entdeckte Erscheinungen, *Phys. Z.* **20**, 401.

Barrington, R. E., and J. S. Belrose, 1963, Preliminary results from the very-low frequency receiver aboard Canada's Alouette satellite, *Nature* **198**, 651.

Brice, N., 1964, Fundamentals of very low frequency emission generation mechanisms, *J. Geophys. Res.* **69**, 4515.

Fahleson, U. V., Theory of electric field measurements conducted in the magnetosphere with electric probes, 1967, *Space Sci. Rev.* **7**, 238.

Fredricks, R. W., C. F. Kennel, F. L. Scarf, G. M. Crook, and I. M. Green, 1968, Detection of electric-field turbulence in the Earth's bow shock, *Phys. Rev. Lett.* **21**, 1761.

Grard, R., C. Nairn, A. Pedersen, S. Klimov, S. Savin, A. Skalsky, and J. G. Trotignon, 1991, Plasma and waves around Mars, *Planet. Space Sci.* **39**, 89.

Gurnett, D. A., Planetary radio emissions, 1992, in Astronomy and Astrophysics Encyclopedia, ed. by S. P. Maran, Van Nostrand Reinhold, 535.

Gurnett, D. A., and L. A. Frank, 1978, Ion acoustic waves in the solar wind, *J. Geophys. Res.* **83**, 58.

Gurnett, D. A., W. S. Kurth, R. L. Poynter, L. J. Granroth, I. H. Cairns, W. M. Macek, S.L. Moses, F. V. Coroniti, C. F. Kennel, and D. D. Barbosa, 1989, First plasma wave observations at Neptune, *Science* **246**, 1494.

Gurnett, D. A., W. S. Kurth, A. Roux, R. Gendrin, C. F. Kennel, and S. J. Bolton, 1991, Lightning and plasma wave observations from the Galileo flyby of Venus, *Science* **253**, 1522.

Gurnett, D. A., W. S. Kurth, and F. L. Scarf, 1979a, Plasma wave observations near Jupiter: Initial Results from Voyager 2, *Science* **206**, 987.

Gurnett, D. A., W. S. Kurth, and F. L. Scarf, 1979b, Auroral hiss observed near the Io plasma torus, *Nature* **280**, 767.

Gurnett, D. A., W. S. Kurth, and F. L. Scarf, 1981, Plasma waves near Saturn: Initial results from Voyager 1, *Science* **212**, 235.

Gurnett, D. A., W. S. Kurth, F. L. Scarf, and R. L. Poynter, 1986, First plasma wave observations at Uranus, *Science* **233**, 106.

Gurnett, D. A., and B. J. O'Brien, 1964, High-latitude geophysical studies with satellite Injun 3, 5. Very-low-frequency radiation, *J. Geophys. Res.* **69**, 65.

Gurnett, D. A., and R. R. Shaw, 1973, Electromagnetic radiation trapped in the magnetosphere above the plasma frequency, *J. Geophys. Res.* **78**, 8136.

Gurnett, D. A., R. R. Shaw, R. R. Anderson, W. S. Kurth, and F. L. Scarf, 1979b, Whistlers observed by Voyager 1: Detection of lightning on Jupiter, *Geophys. Res. Lett.* **6**, 511.

Jones, D., 1980, Latitudinal beaming of planetary radio emissions, *Nature* **288**, 225.

Kennel, C. F., F. L. Scarf, R. W. Fredricks, J. H. McGehee, and F. V. Coroniti, 1970, VLF electric field observations in the magnetosphere, *J. Geophys. Res.* **75**, 6136.

Kennel, C. F., and H. E. Petschek, 1966, Limit on stably trapped particle fluxes, *J. Geophys. Res.* **71**,1.

Kindel, J. M., and C. F. Kennel, 1971, Topside current instabilities, *J. Geophys. Res.* **76**, 3055.

Kintner, P. M., and D. A. Gurnett, 1977, Observations of ion cyclotron waves within the plasmasphere by Hawkeye 1, *J. Geophys. Res.* **82**, 2314.

Kintner, P. M., M. C. Kelley, and F. S. Mozer, 1978, Electrostatic hydrogen cyclotron waves near one Earth radius altitude in the polar magnetosphere, *Geophys. Res. Lett.* **5**, 139.

Krall, N. A., and A. W. Trivelpiece, 1973, *Principles of Plasma Physics*, McGraw-Hill, New York.

Kurth, W. S., 1991, Continuum radiation in planetary magnetospheres, Planetary Radio Emissions III, Ed. by H. O. Rucker, S. J. Bauer, and M. L. Kaiser, Verlage der Osterreichischen Akademie der Wissenschaften, Wein, Austria, 329.

Kurth, W. S., and D. A. Gurnett, 1991, Plasma waves in planetary magnetospheres, *J. Geophys. Res.* **96**, 18,877.

Melrose, D. B., 1981, A theory for the nonthermal radio continuum in the terrestrial and Jovian magnetospheres, *J. Geophys. Res.* **86**, 30.

Roux, A., S. Perraut, J. L. Rauch, C. deVilledarg, G. Kremser, A. Korth, and D. T. Young, 1982, Wave-particle interactions near ω_{He+} observed on board Geos 1 and 2, 2. Generation of ion cyclotron waves and heating of He^+ ions, *J. Geophys. Res.* **87**, 8174.

Scarf, F. L., R. W. Fredricks, L. A. Frank, and M. Neugebauer, 1971, Nonthermal electrons da high-frequency waves in the upstream solar wind, 1. Observations, *J. Geophys. Res.* 76, 5162.

Scarf, F. L., R. W. Fredricks, L. A. Frank, C. T. Russell, P. J. Coleman, Jr., and M. Neugebauer, 1970, Direct correlations of large amplitude waves with suprathermal protons in the upstream solar wind, *J. Geophys. Res.* **75**, 7316.

Scarf, F. L., D. A. Gurnett, and W. S. Kurth, 1979a, Jupiter plasma wave observations: An initial Voyager 1 overview, *Science* **204**, 991.

Scarf, F. L., D. A. Gurnett, W. S. Kurth, and R. L. Poynter, 1982, Voyager 2 plasma wave observations at Saturn, *Science* **215**, 587.

Scarf, F. L., W. W. L. Taylor, and I. M. Green, 1979b, Plasma waves near Venus: Initial observations, *Science* **203**, 748.

Scudder, J. D., A. Mangeney, C. Lacome, C. C. Harvey, C S. Wu, and R. R. Anderson, 1986, The resolved layer of a collisionless, high β, supercritical, quasi-perpendicular shock wave, 3. Vlasov electrodynamics, *J. Geophys. Res.* **91**, 11,075.

Shaw, R. R., and D. A. Gurnett, 1975, Electrostatic noise bands associated with the electron gyrofrequency and plasma frequency in the outer magnetosphere, *J. Geophys. Res.* **80**, 4259.

Stix, T., 1962, *The Theory of Plasma Waves*, McGraw-Hill, N. York, 110.

Stone, R. G., B. M. Pedersen, C. C. Harvey, P. Canu, N. Cornilleau-Wehrlin, M. D. Desch, C. deVilledary, J. Fainberg, W. M. Farrell, K. Goetz, R. A. Hess, S. Hoang, M. L. Kaiser, P. J. Kellogg, A. Lecacheux, N. Lin, R. J. MacDowall, R. Manning, C. A. Meetre, N. Meyer-Vernet, M. Moncuquet, V. Osherovich, M. J. Reiner, A. Tekle, J. Thiessen, and P. Zarka, 1992, Ulysses Radio and plasma wave observations in the Jupiter Environment, *Science* **257**, 1524.

Storey, L. R. O., 1953, An investigation of whistling atmospherics, *Phil. Trans. Roy. Soc.* (London) **A 46**, 113.

Taylor, W. W. L., B. K. Parady, and L. J. Cahill, Jr., 1975, Explorer 45 observations of 1- to 30-Hz magnetic fields during magnetic storms, *J. Geophys. Res.* **80**, 1271.

Thorne, R. M., and J. Moses, 1983, Electromagnetic ion-cyclotron instability in the multi-ion Jovian magnetosphere, *Geophys. Res. Lett.* **10**, 631.

Thorne, R. M., and F. L. Scarf, 1984, Voyager 1 evidence for ion-cyclotron instability in the vicinity of the Io plasma torus, *Geophys. Res. Lett.* **11**, 263.

Table 1

Plasma wave mode	Frequency range	Electromagnetic/ electrostatic	Polarization	Free energy source
Free-space (L,O) mode	$\omega > \omega_{pe}$	Electromagnetic	L	Beam, loss cone
Free-space (R,X) mode	$\omega > \omega_{R=0}$	Electromagnetic	R	Beam, loss cone
Electron plasma oscillations (Langmuir waves)	$\omega \simeq \omega_{pe}$	Electrostatic	-	Beam
Z mode	$\omega_{UHR} > \omega > \omega_{L=0}$	Electromagnetic, electrostatic near ω_{UHR}	R for $\omega > \omega_{pe}$ L for $\omega < \omega_{pe}$	Beam
Electron cyclotron waves	Bands near $\omega \simeq (n + 1/2)\omega_{ce}$	Electrostatic	-	Ring distribution (electrons)
Whistler mode	$\omega < \text{Min}\{\omega_{ce}, \omega_{pe}\}$	Electromagnetic, electrostatic near ω_{LHR}	R	Loss cone, beam above ω_{LHR}
Ion-acoustic mode	$\omega \lesssim \omega_{pi}$	Electrostatic	-	Drift between electrons and ions
Electrostatic ion cyclotron waves	Bands near $\omega \simeq (n + 1/2)\omega_{ci}$	Electrostatic	-	Ring distribution (ions), field-aligned currents
Electromagnetic ion cyclotron waves	$\omega << \omega_{ci}$	Electromagnetic	L	Pressure anisotropies

NOTE: $\omega_{R=0} = \omega_{ce}/2 + \sqrt{(\omega_{ce}/2)^2 + \omega_{pe}^2}$ $\qquad \omega_{UHR} = \sqrt{\omega_{ce}^2 + \omega_{pe}^2}$

$\omega_{L=0} = -\omega_{ce}/2 + \sqrt{(\omega_{ce}/2)^2 + \omega_{pe}^2}$ $\qquad \omega_{LHR} \simeq \sqrt{\omega_{ce}\,\omega_{ci}}$, if $\omega_{pe} \gg \omega_{ce}$

Table 2

Type of Plasma Wave	Venus	Earth	Mars	Jupiter	Saturn	Uranus	Neptune
Upstream electron plasma oscillations	X	X	X	X	X	X	X
Upstream ion acoustic waves		X	X	X			
Electrostatic noise at the bow shock	X	X	X	X	X	X	X
Electron cyclotron harmonic waves		X		X	X	X	X
Upper hybrid resonance waves		X		X	X	X	X
Whistler-mode hiss		X		X	X	X	X(?)
Whistler-mode chorus		X		X	X	X	
Whistler-mode auroral hiss		X		X			
Electrostatic ion cyclotron waves		X		X(?)			X(?)
Ion cyclotron whistlers (lightning)		X					
Electromagnetic ion cyclotron emissions		X		X			X(?)

FIGURE CAPTIONS

Figure 1. A typical antenna geometry for detecting space plasma waves. Electric fields are usually detected by an electric dipole antenna, and magnetic fields are detected by either a loop antenna or a search coil magnetometer.

Figure 2. A block diagram of a typical plasma wave instrument. These instruments often consist of an onboard spectrum analyzer which gives low-resolution continuous spectrums, and a wideband waveform receiver which gives very high-resolution spectrums for selected intervals.

Figure 3. A sketch of the various boundaries and regions that occur in the solar wind upstream of a planet. Since the solar wind is supersonic, a shock wave forms upstream of the planet. Electrons and ions energized at the shock escape upstream into regions known as the electron foreshock and the ion foreshock.

Figure 4. An example of electron plasma oscillations in the solar wind upstream of Jupiter. These waves occur in the electron foreshock and are produced by energetic ($\sim$ 1 to 10 keV) electron beams streaming into the solar wind from the bow shock.

Figure 5. A high-resolution frequency-time spectrogram of ion-acoustic waves observed in the solar wind upstream of the Earth's magnetosphere. These waves are produced by energetic ($\sim$ 10 keV) ions streaming into the solar wind from the bow shock.

Figure 6. The Voyager 1 inbound crossing of Jupiter's bow shock. An abrupt burst of broadband electric field noise can be seen at the shock. This noise is believed to be caused by ion beams gyrating back into the solar wind from the shock. Electron plasma oscillations can also be seen upstream of the shock.

Figure 7. The inbound Voyager 1 crossing of Jupiter's magnetopause. The intense band of noise from about 2 to 7 kHz is continuum radiation trapped in the low-density magnetospheric

cavity. The low-frequency cutoff of the continuum radiation is at the electron plasma frequency, f_{pe}.

Figure 8. An example of electrostatic electron cyclotron harmonic (ECH) waves in Saturn's magnetosphere. These emissions occur in narrow bands slightly above harmonics of the electron cyclotron frequency, f_{ce}.

Figure 9. An example of upper hybrid resonance (UHR) emissions in Jupiter's magnetosphere. These emissions occur in narrow bands near the upper hybrid resonance frequency, f_{UHR}.

Figure 10. The upper panel shows electric field intensities observed during the Voyager 1 pass through the inner region of the Jovian magnetosphere. The lower panel shows the magnetic latitude. Both ECH and UHR waves always occur very close to the magnetic equator.

Figure 11. The top panel shows an electric field spectrum of whistler-mode hiss and chorus emissions in Jupiter's Io torus. The bottom panel shows the energy, $W_{\parallel}$, of electrons that are in cyclotron resonance with these waves. The hiss tends to interact with very energetic electrons ($\sim$ 100 to 1000 keV), whereas the chorus interacts with much lower energies ($\sim$ 1 to 10 keV).

Figure 12. A high-resolution frequency-time spectrogram of chorus emissions. These emissions are highly structured and often consist of narrowband tones rising in frequency with increasing time. Chorus often has a sharp notch in the spectrum at one-half of the electron cyclotron frequency, $f_{ce}/2$.

Figure 13. An electric field spectrum of electrostatic ion cyclotron waves observed in the Earth's magnetosphere by the S3-3 spacecraft [Kintner et al., 1979]. These waves occur between harmonics of the proton cyclotron frequency ($f_{cH}+$) and are driven by currents flowing along the auroral field lines.

A-G93-51

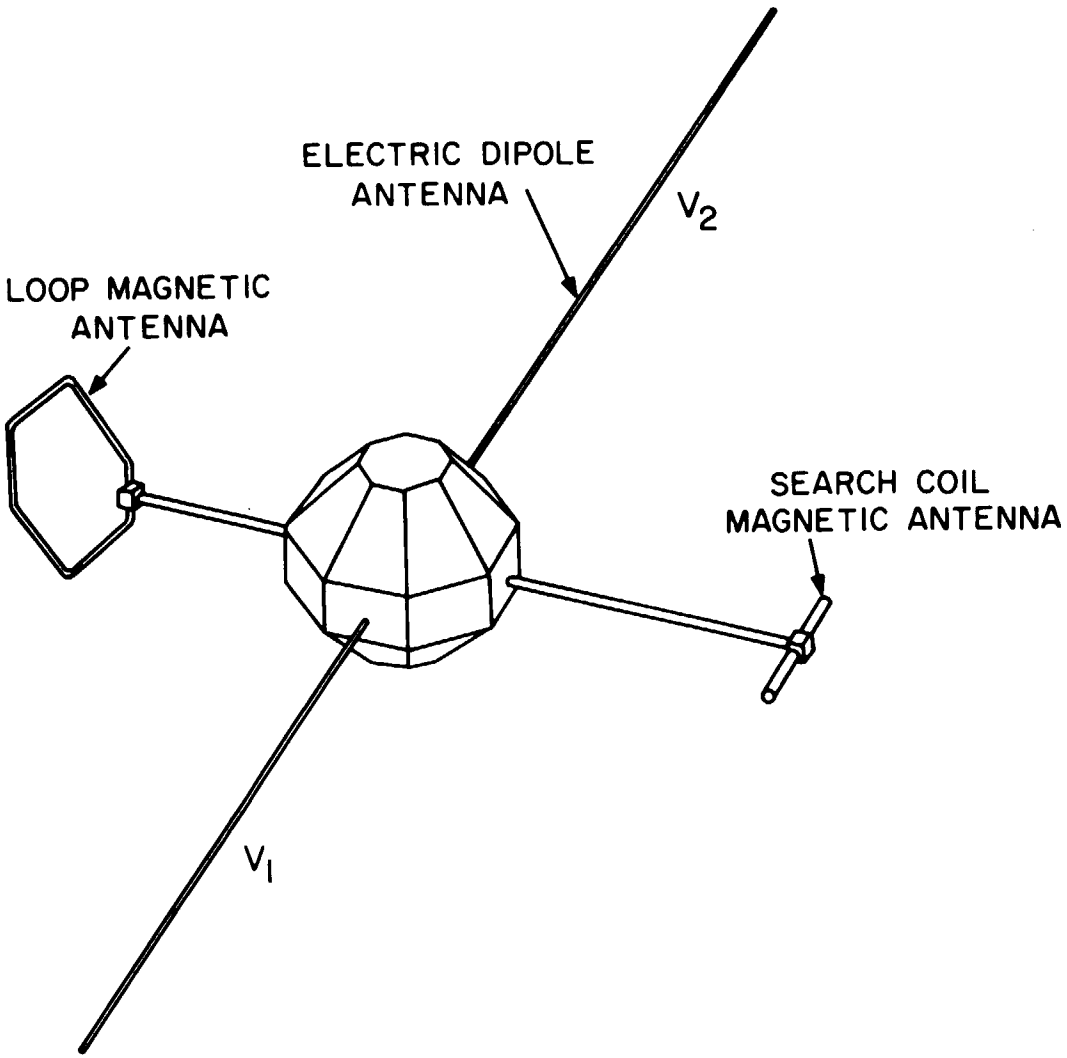
ELECTRIC DIPOLE
ANTENNA
V_2
LOOP MAGNETIC
ANTENNA
SEARCH COIL
MAGNETIC ANTENNA
V_1

Fig. 1

A-G93-52

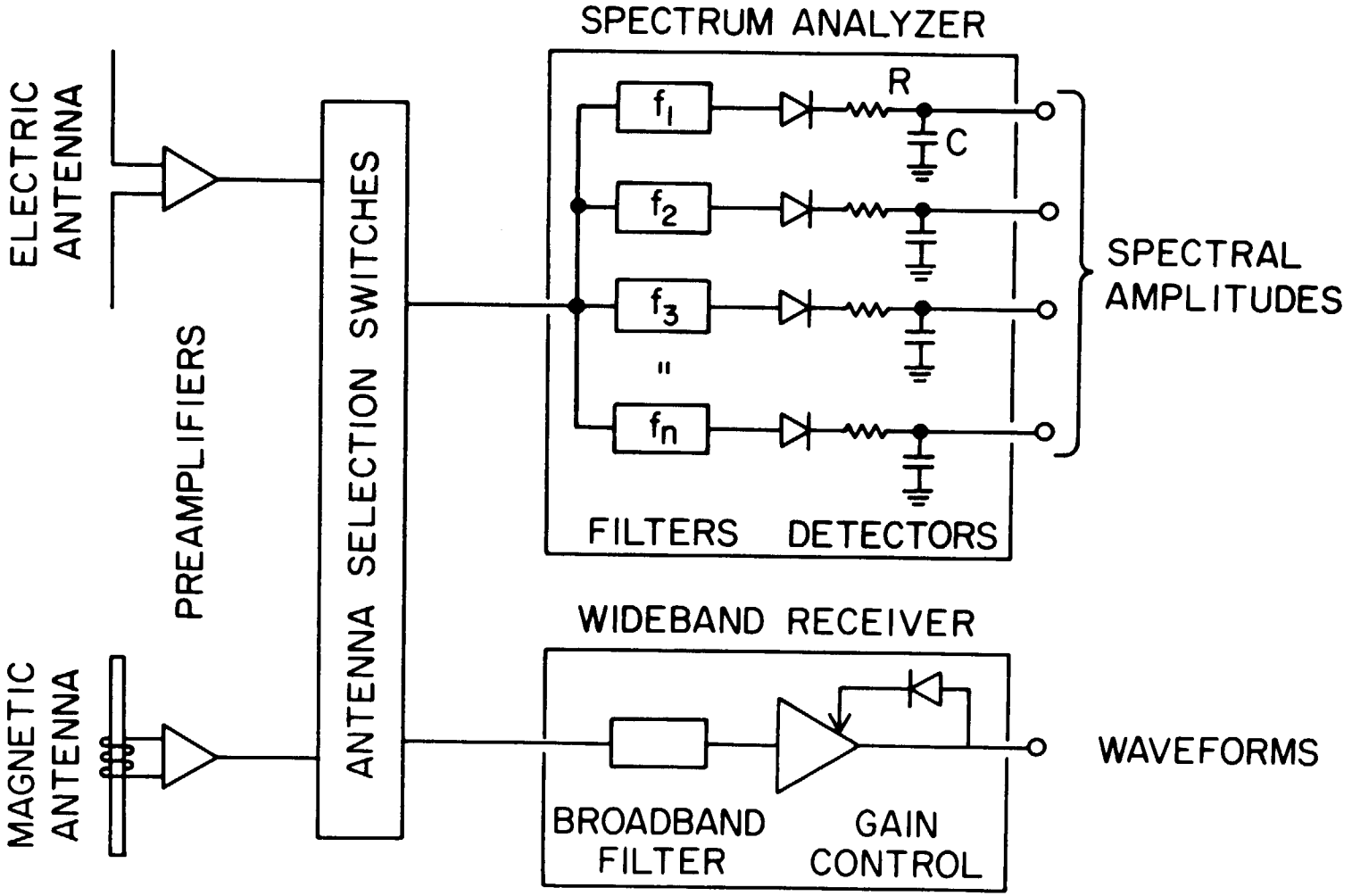
SPECTRUM ANALYZER
ELECTRIC ANTENNA
PREAMPLIFIERS
ANTENNA SELECTION SWITCHES
R
C
f_1
f_2
f_3
f_n
SPECTRAL AMPLITUDES
FILTERS
DETECTORS
WIDEBAND RECEIVER
MAGNETIC ANTENNA
BROADBAND FILTER
GAIN CONTROL
WAVEFORMS

Fig. 2

A-G93-24-1

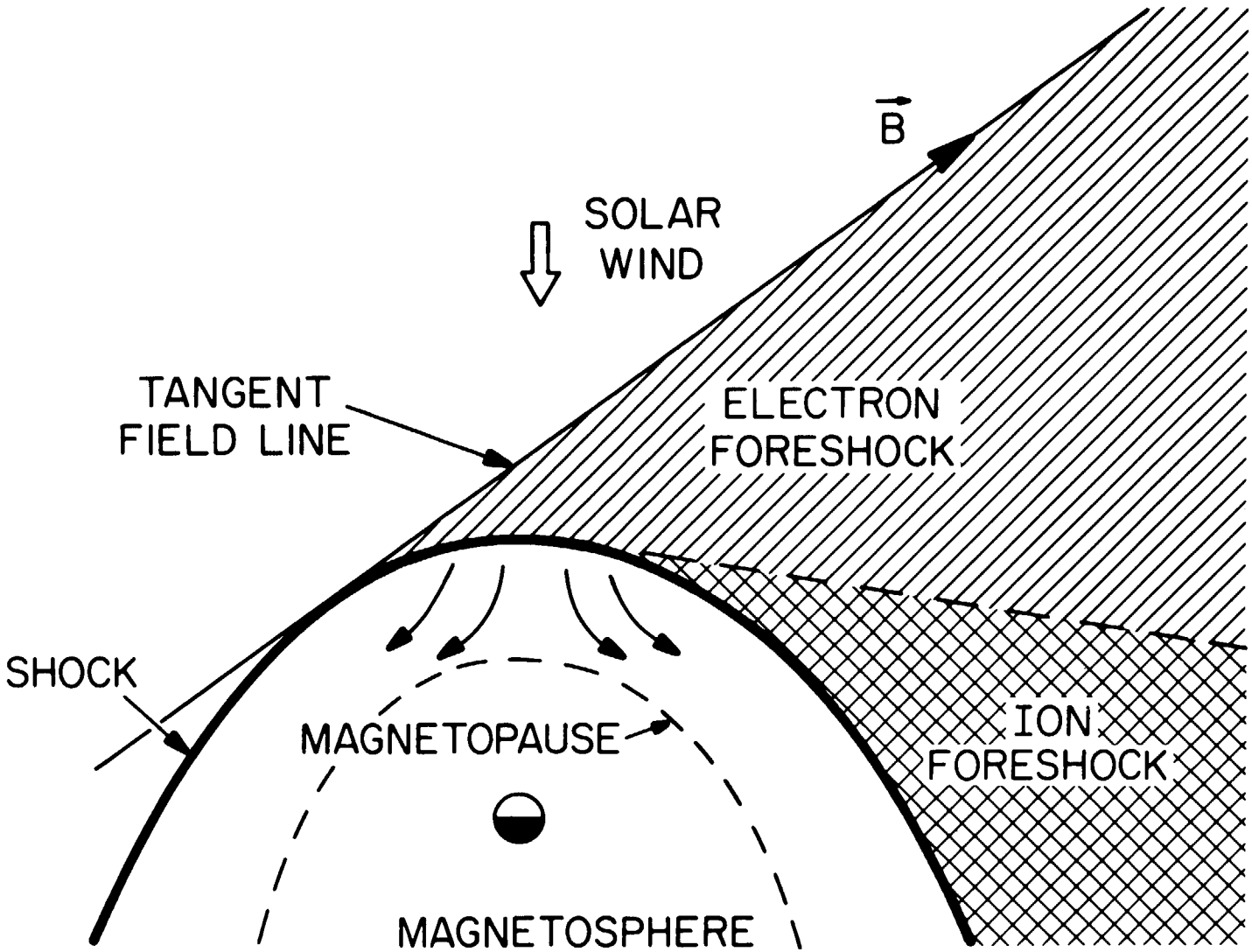

Fig. 3

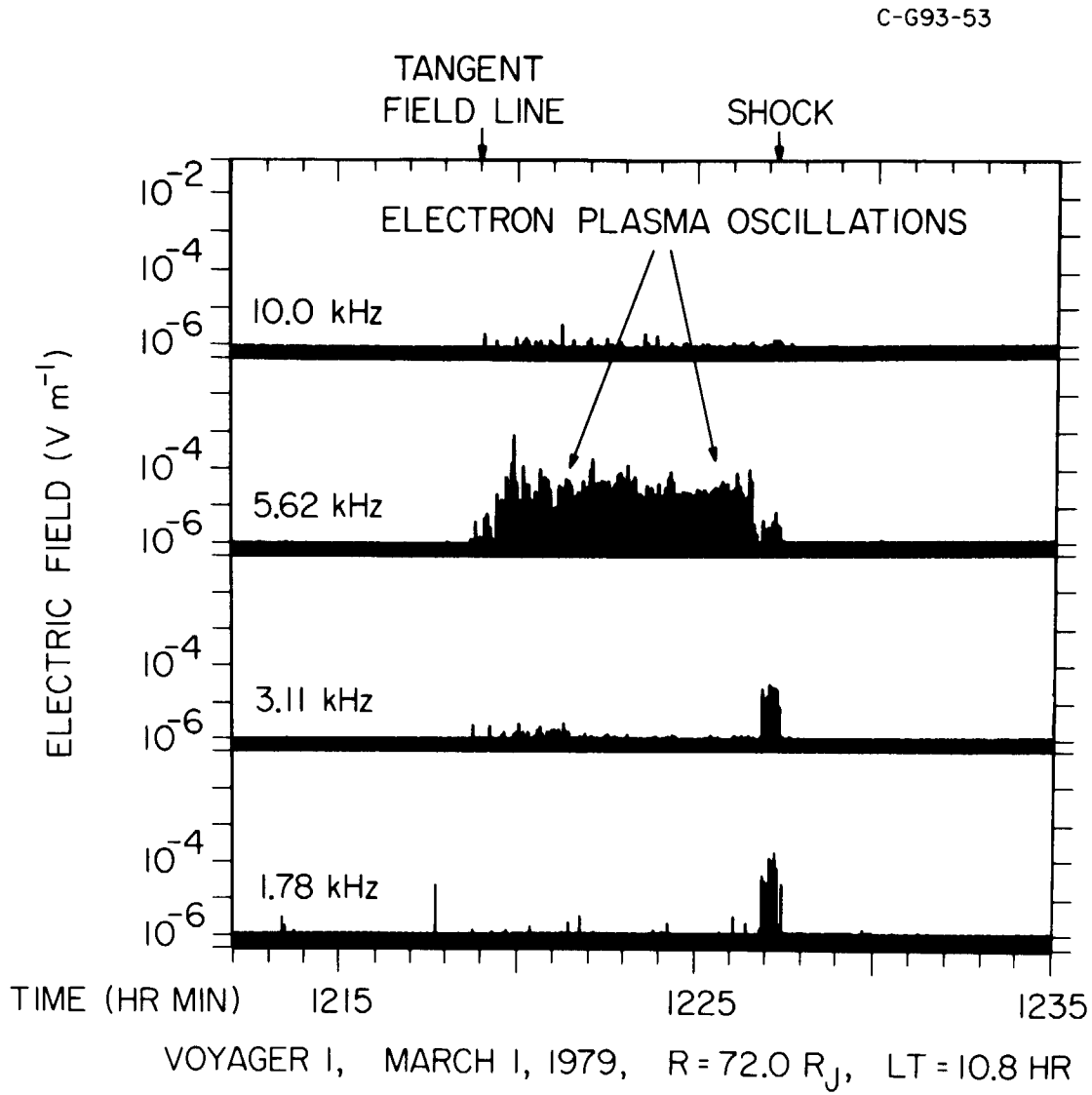
C-G93-53
TANGENT
FIELD LINE
SHOCK
ELECTRON PLASMA OSCILLATIONS
10.0 kHz
5.62 kHz
3.11 kHz
1.78 kHz
ELECTRIC FIELD (V m⁻¹)
10⁻²
10⁻⁴
10⁻⁶
TIME (HR MIN)
1215
1225
1235
VOYAGER 1, MARCH 1, 1979, R = 72.0 R_J, LT = 10.8 HR

Fig. 4

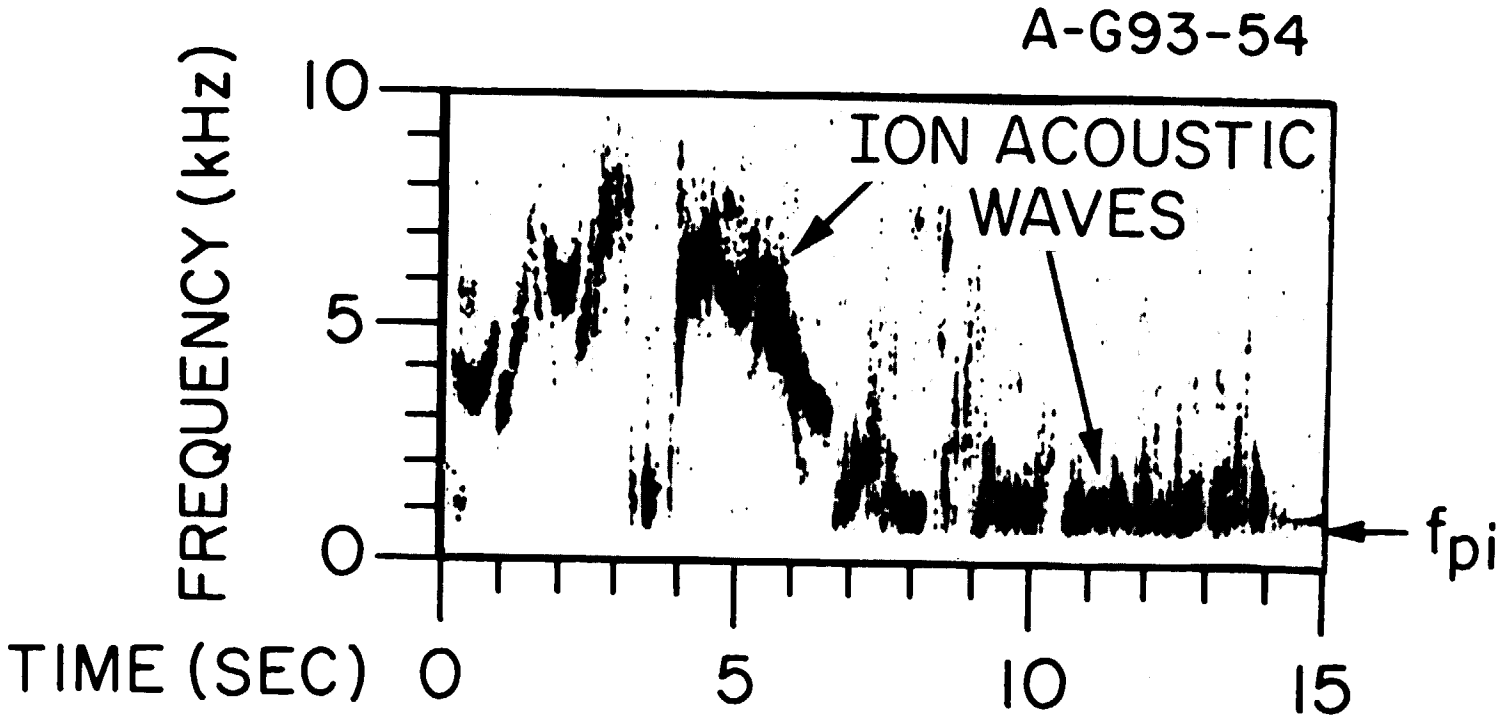

ISEE-1, NOV 8, 1977, 2022:15 UT

R = 17.1 R_E LT = 8.4 HR

Fig. 5

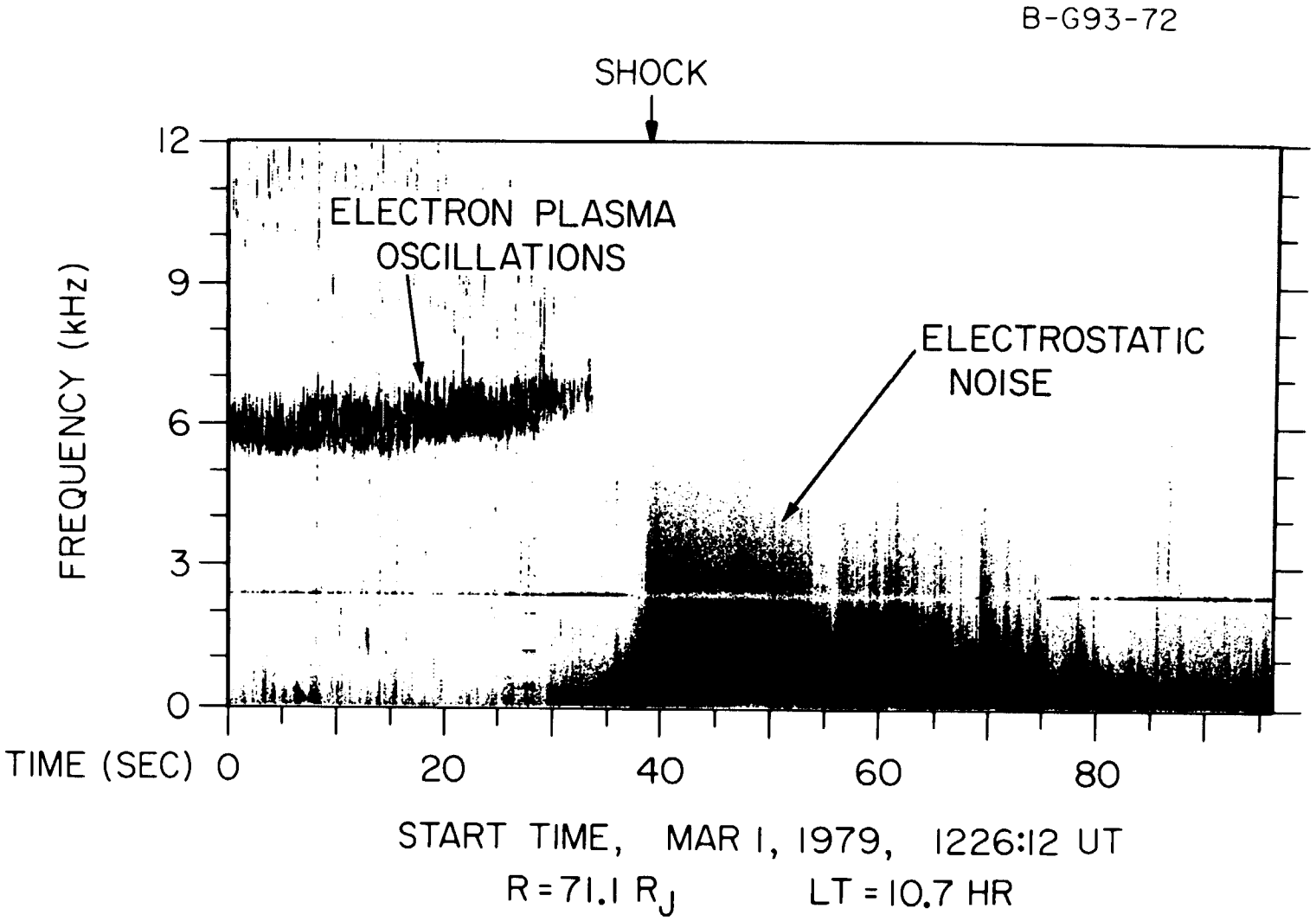
B-G93-72
SHOCK
ELECTRON PLASMA
OSCILLATIONS
ELECTROSTATIC
NOISE
FREQUENCY (kHz)
12
9
6
3
0
TIME (SEC) 0
20
40
60
80
START TIME, MAR 1, 1979, 1226:12 UT
R = 71.1 R_J
LT = 10.7 HR

Fig. 6

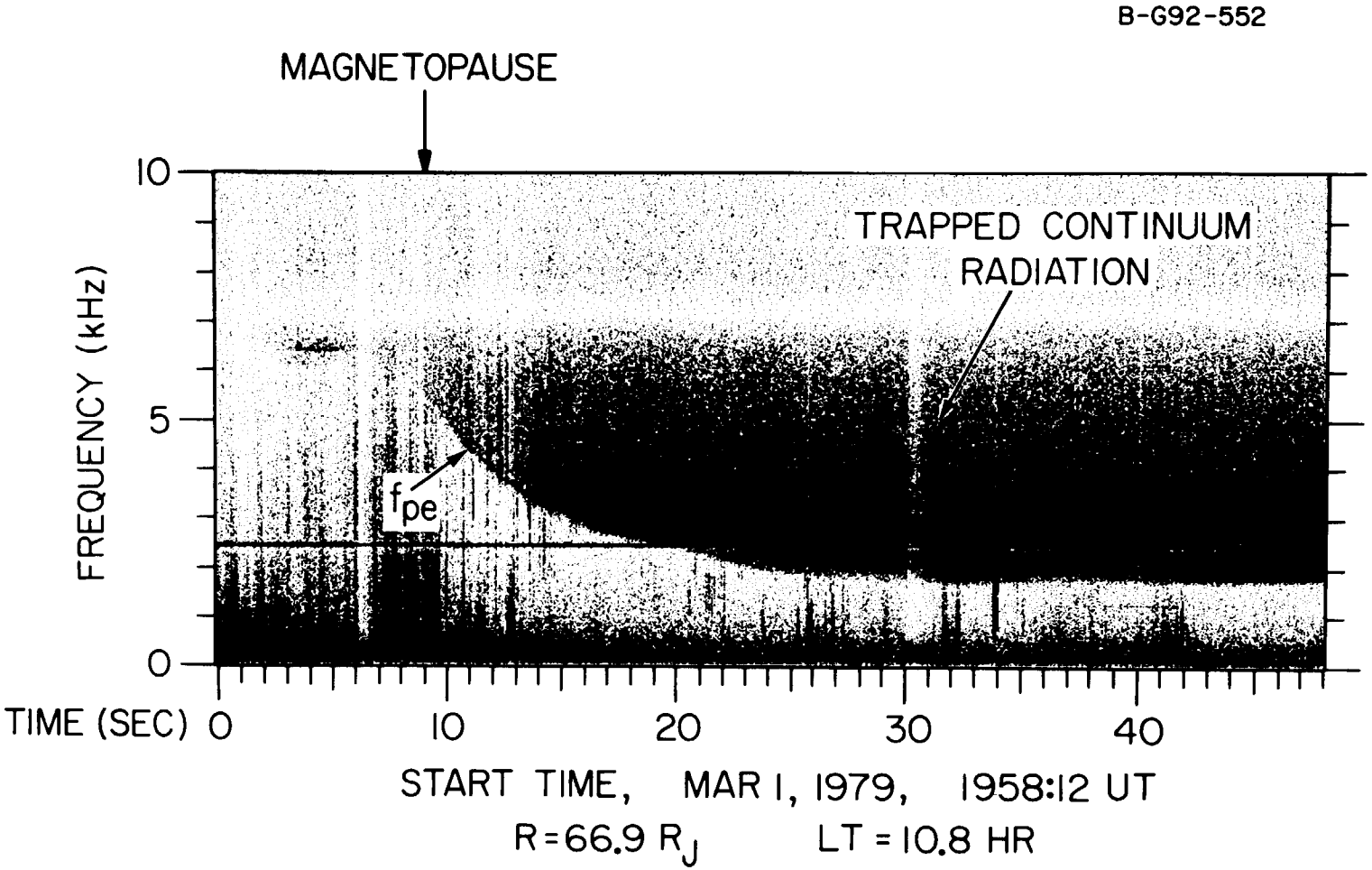
B-G92-552
MAGNETOPAUSE
10
5
0
FREQUENCY (kHz)
TRAPPED CONTINUUM
RADIATION
f_{pe}
TIME (SEC) 0
10
20
30
40
START TIME, MAR 1, 1979, 1958:12 UT
R=66.9 R_J
LT = 10.8 HR

Fig. 7

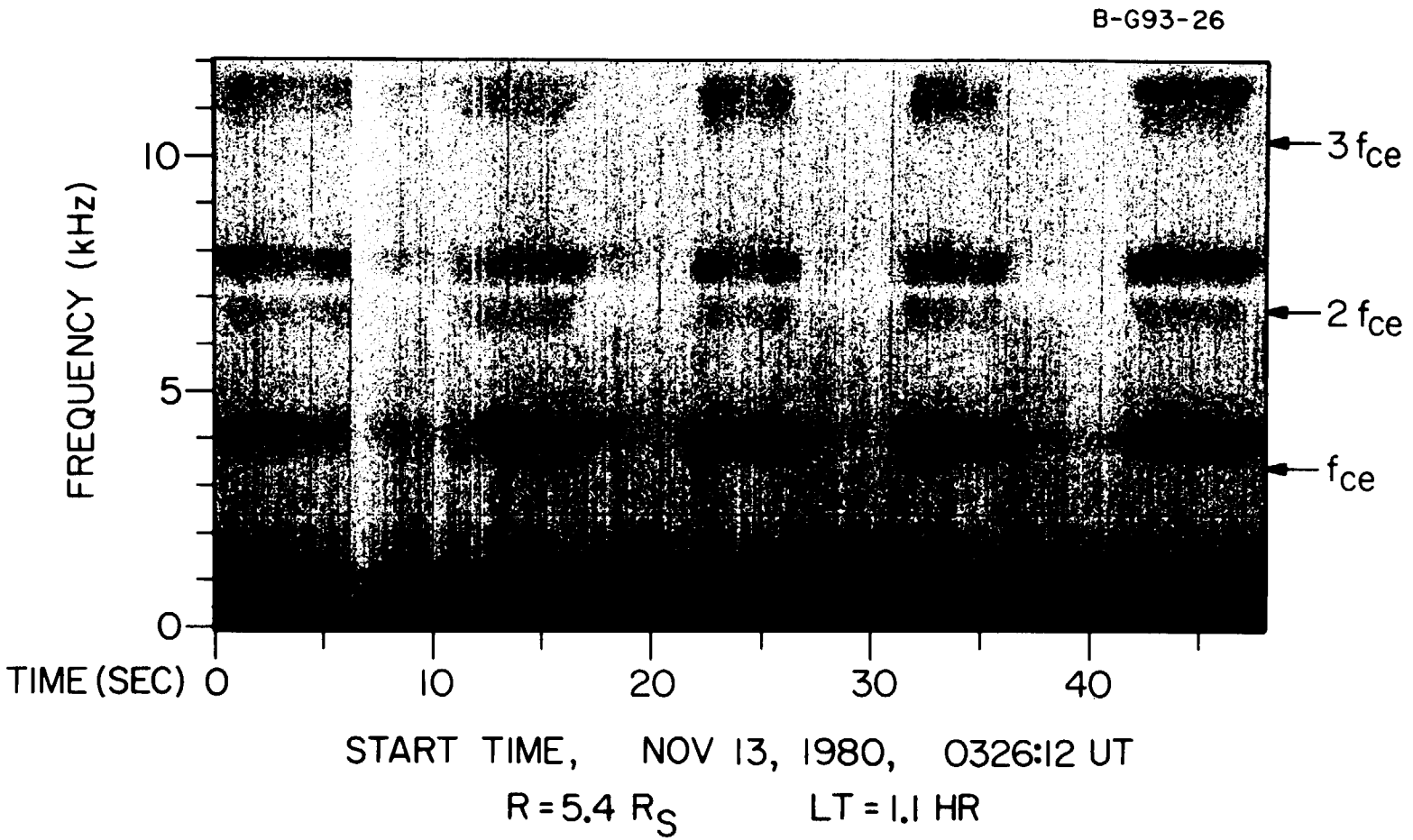
B-G93-26
FREQUENCY (kHz)
10
5
0
3 fce
2 fce
fce
TIME (SEC) 0
10
20
30
40
START TIME, NOV 13, 1980, 0326:12 UT
R = 5.4 RS
LT = 1.1 HR

Fig. 8

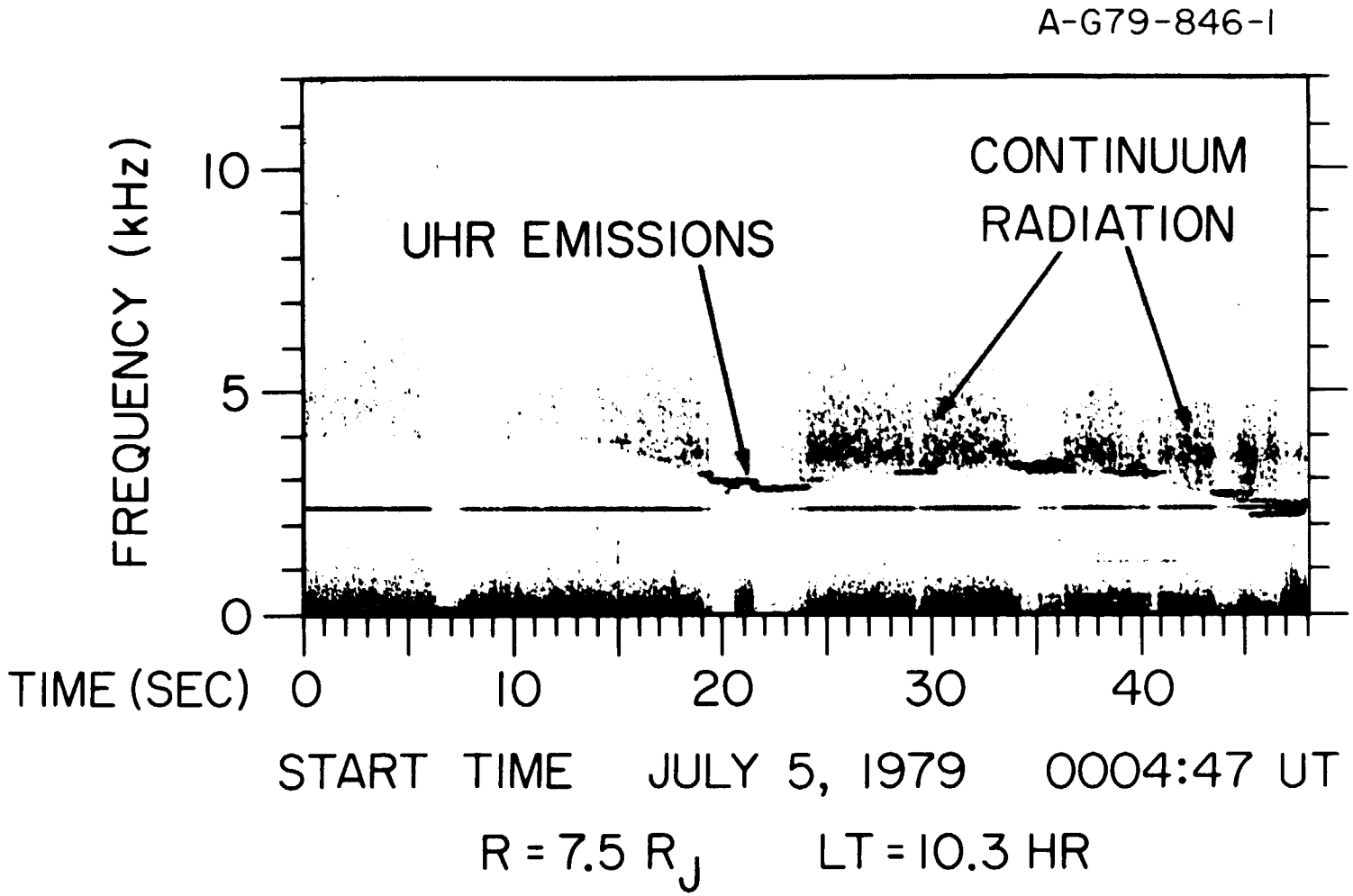
A-G79-846-1
FREQUENCY (kHz)
10
5
0
UHR EMISSIONS
CONTINUUM
RADIATION
TIME (SEC)
0
10
20
30
40
START TIME JULY 5, 1979 0004:47 UT
R = 7.5 R_J
LT = 10.3 HR

Fig. 9

C-G79-864-5

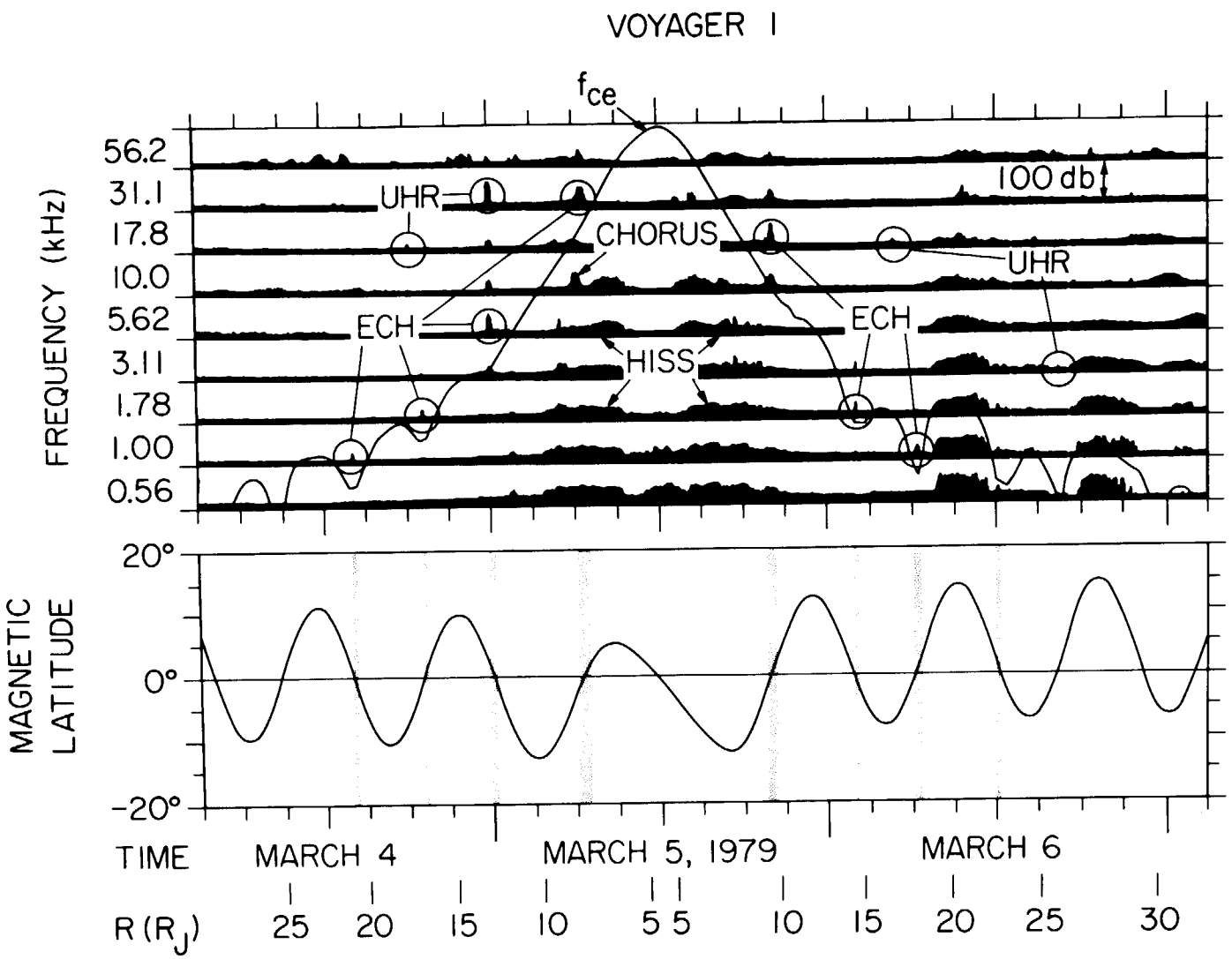

Fig. 10

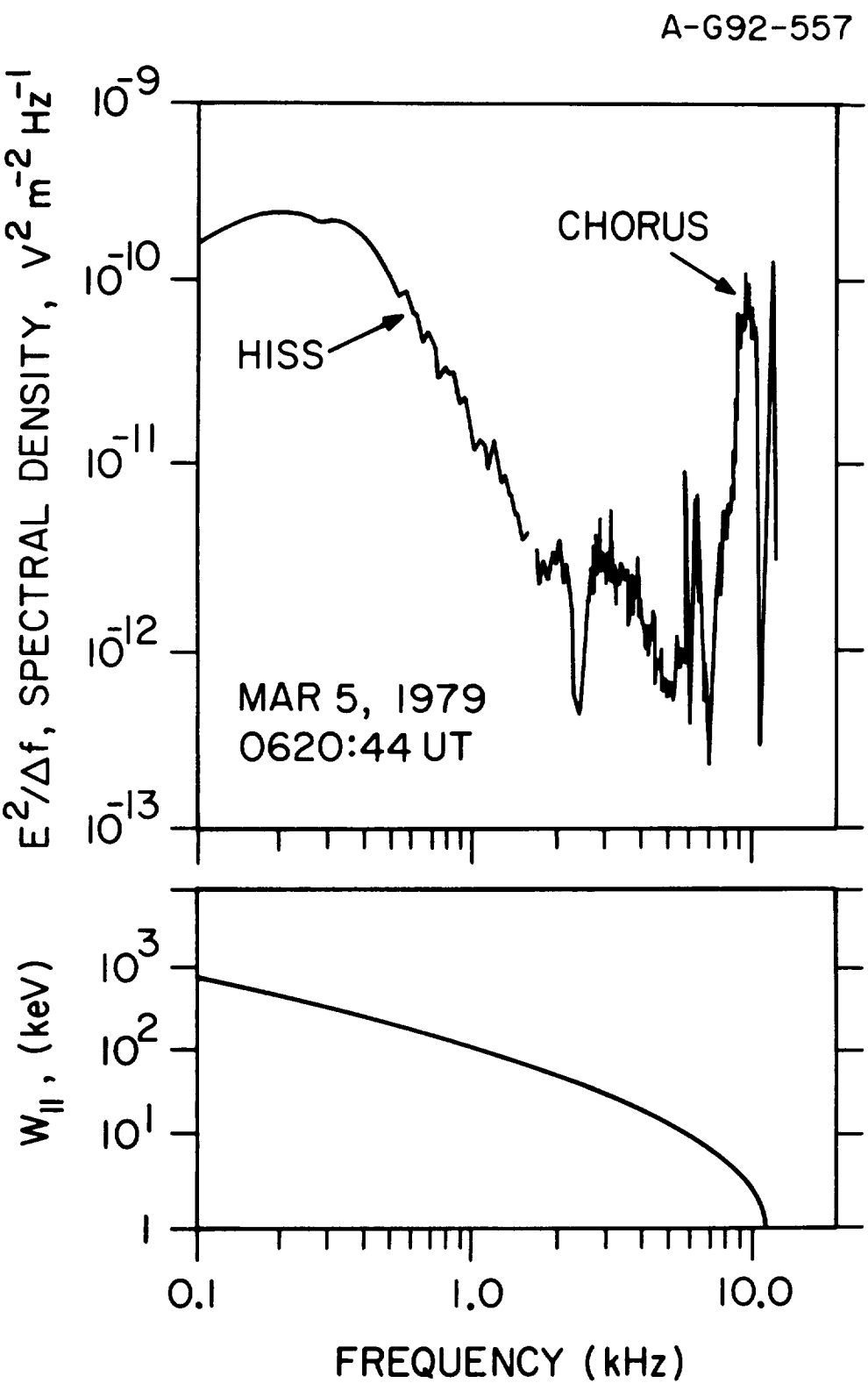
A-G92-557
$E^2/\Delta f$, SPECTRAL DENSITY, $V^2 m^{-2} Hz^{-1}$
10^{-9}
10^{-10}
10^{-11}
10^{-12}
10^{-13}
CHORUS
HISS
MAR 5, 1979
0620:44 UT
$W_{||}$, (keV)
10^3
10^2
10^1
1
0.1
1.0
10.0
FREQUENCY (kHz)

Fig. 11

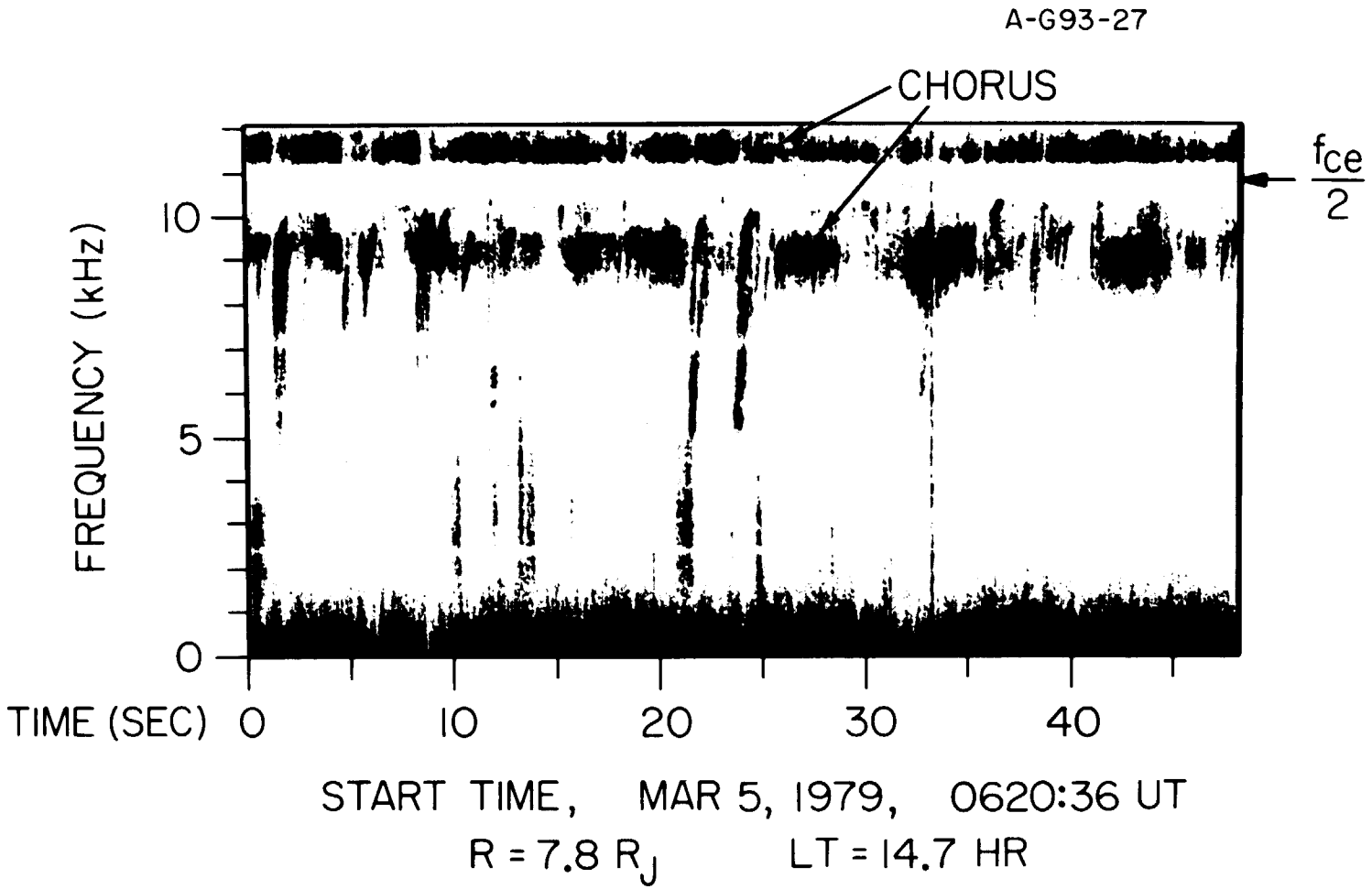
A-G93-27
CHORUS
f_{ce}
2
FREQUENCY (kHz)
10
5
0
TIME (SEC) 0
10
20
30
40
START TIME, MAR 5, 1979, 0620:36 UT
R = 7.8 R_J
LT = 14.7 HR

Fig. 12

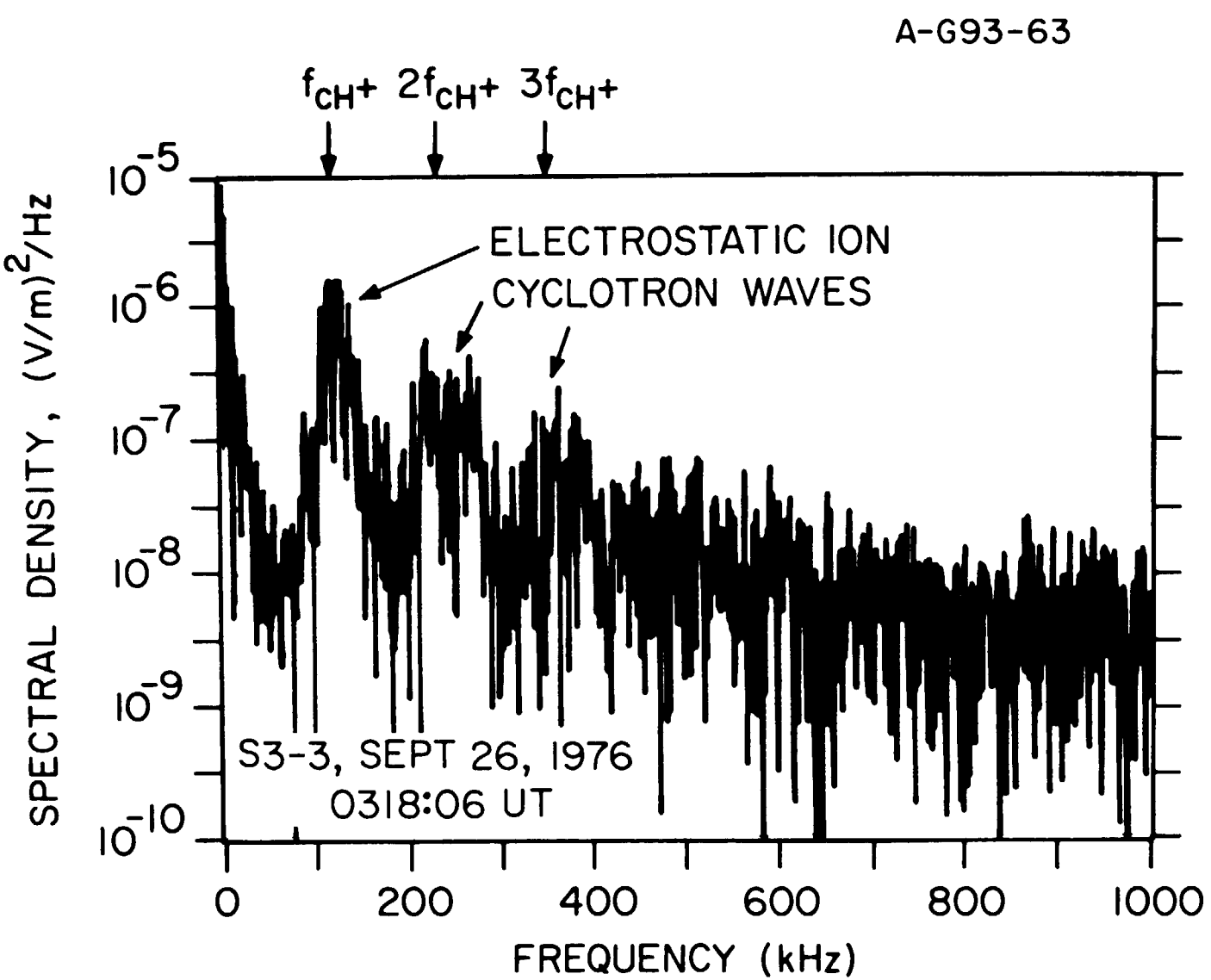
A-G93-63
f_{CH+} $2f_{CH+}$ $3f_{CH+}$
ELECTROSTATIC ION
CYCLOTRON WAVES
S3-3, SEPT 26, 1976
0318:06 UT
SPECTRAL DENSITY, $(V/m)^2/Hz$
10^{-5}
10^{-6}
10^{-7}
10^{-8}
10^{-9}
10^{-10}
0
200
400
600
800
1000
FREQUENCY (kHz)

Fig. 13